Computational Condensed Matter 36 (2023) e00821

Contents lists available at ScienceDirect

Computational Condensed Matter

journal homepage: www.elsevier.com/locate/cocom

Unveiling the mechanical and dynamical stability to the contribution of transport properties of FeNbSb: A first principle approach

O.C. Olawole [a], B.I. Adetunji [b], P.O. Adebambo [c,*], G.A. Adebayo [c]

[a] Department of Physics, Covenant University, Ogun State, Nigeria
[b] Department of Physics, Bells University of Technology, Ota, 23401, Nigeria
[c] Department of Physics, Federal University of Agriculture, PMB 2240, Abeokuta, Nigeria

A B S T R A C T

This study adopts first principle calculations to probe the electronic, elastic, vibrational, and transport properties of FeNbSb Alloys. The elastic and phonon properties were deduced to explain the stability and dynamical nature of FeNbSb alloy. Voigt-Reuss-Hill approximation was used for the mechanical properties, Poisson's ratio for brittleness, while Pugh's rule was used to estimate the alloy ductility. Besides, the absence of negative frequency revealed the dynamical stability of FeNbSb. Also, the thermal conductivity, electrical conductivity, power factor, and Seebeck coefficient were estimated in terms of energy relative to the Fermi level at 300 $K \leq T \leq$ 800 K. The study achieved a power factor of 15×10^{11} $\mu W/cmK^2s$ and a maximum zT of 0.52 at 800 K for *FeNbSb*. In conclusion, the result of this study suggests that FeNbSb p-type is a suitable material for thermoelectricity.

1. Introduction

Thermoelectric devices, which are sustainable, cost-effective, and eco-friendly, as depicted in Fig. 1, are fast-growing alternative energy technology in addressing the world's energy crisis [1–3]. It comprised heavily doped n- and p-type semiconductors coupled thermally in parallel and electrically in series. These immaculate energy conversions of waste heat to electricity are the favourite of scholars in the energy field due to their noiseless nature, absence of mechanically moving parts, and durability [4,5]. Despite the promising nature of the thermoelectric device, its conversion efficiency (η) is limited due to the high Carnot efficiency (η_c), and the low figure of merit zT [6]. The formal limitation requires material devices that can withstand higher temperatures greater than 1000 K while the latter solves with a high power factor $(S^2\sigma)$ and low lattice thermal conductivity (k_l). Though researchers have enhanced the $S^2\sigma$ of the thermoelectric device through the tuning of its electrical transport properties and band convergence [7,8], quantum confinement [9], and deep state doping [10,11]. Also, structural modifications through porosity layout [12], grain purification [13,14], and the presence of residues [15] have been used to achieve low k_l. However, in addressing these concerns, researchers have been studying half-Heusler alloys (ternary semiconducting/metallic materials having either 1:1:1 or 2:1:1) [16,17] as suitable materials for achieving both high η_c and zT (a higher energy conversion efficiency) due to their narrow bandgaps [18], substantial mechanical properties, sizeable electrical conductivity, robust thermal stability, and higher power factor [16,19–28].

The primary aim of this work is to investigate the electronic, mechanical, dynamical, and thermoelectric properties of Bulk FeNbSb. It is essential to provide a template to improve the thermoelectric properties of FeNbSb HH alloy. Other sections in this work are organized as follows: Section 2 has the Theoretical Background and Computational procedure, while our Findings are discussed in section 3. Finally, we provided our principal conclusions in section 4.

2. Theoretical Background and Computational procedure

Thermoelectric technology is dependent on its figure of merit (zT) [29] as stated in Equation (1)

$$zT = \left(\frac{S^2\sigma}{k_e + k_l}\right)T \tag{1}$$

where S (VK^{-1}) typifies the Seebeck coefficient, σ (Sm^{-1}) is the electrical conductivity, k $(Wm^{-1}K^{-1})$ represents thermal conductivity, T (K) denotes the absolute working temperature, k_e refers to the electronic thermal conductivity and k_l is known as the lattice thermal conductivity [30,31].

Interestingly, its maximum efficiency (η_{max}), maximum output power (P_{max}), and the power factor (PF) can be computed from Equations (2)–

* Corresponding author.
E-mail address: adebambo@physics.unaab.edu.ng (P.O. Adebambo).

https://doi.org/10.1016/j.cocom.2023.e00821
Received 24 February 2023; Received in revised form 31 May 2023; Accepted 1 June 2023
Available online 2 June 2023

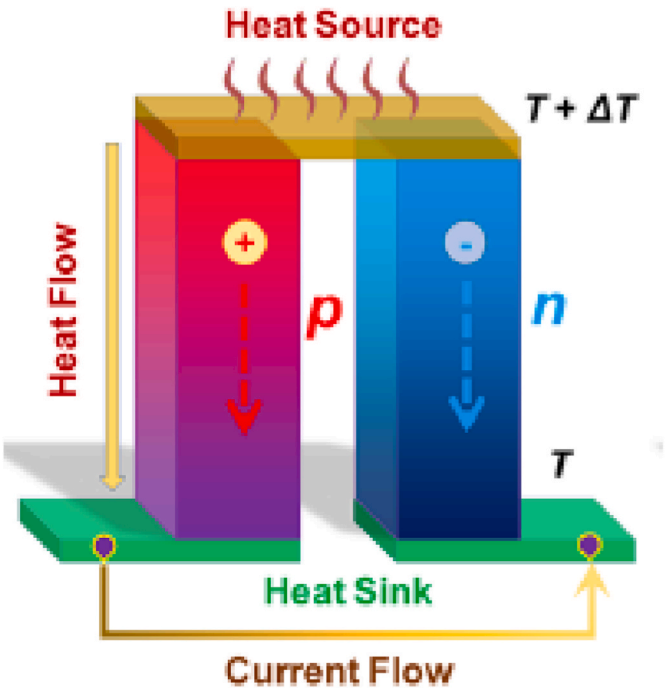

Fig. 1. Thermoelectric configuration of P and N-types [1].

(4) as

$$\eta_{max} = \left(\frac{T_h - T_c}{T_h}\right)\left(\frac{\sqrt{1+z\underline{T}}-1}{\sqrt{1+z\underline{T}}+\frac{T_c}{T_h}}\right) \tag{2}$$

$$P_{max} = \frac{S^2\Delta T^2}{4R} \tag{3}$$

$$PF = S^2\sigma \tag{4}$$

where T_h is the hot-side temperature and T_c represents the cold-side temperature, R depicts the total resistance and $\underline{T}$ connotes the average temperature of T_h and T_c of the device engine.

This study adopts the first principle calculations and the semi-classical Boltzmann transport theory to examine the electronic structure, transport phenomena, and TE properties of FeNbSb materials that would thereafter serve as a theoretical benchmark for upgrading the power factor of the FeNbSb device.

The study performed the first principle calculations via the Quantum Espresso package [32]. Also, the study used PBEsol exchange-correlation functional within the generalized gradient approximation (GGA) [33] that produced the lattice constant of FeNbSb as 5.89 $\dot{A}$. In addition, a plane-wave basis set was adopted with a kinetic energy cutoff of 50 R_y and charge density of 500 R_y. These values are higher enough to get converged results. The k-mesh applied in the first irreducible Brillouin zone was $12 \times 12 \times 12$, which was generated with the MonkhorstePack scheme [34]. The study implemented the Voigt [35], Reuss [36], and Hill [37] average methods for the calculation of the system elastic constants (bulk modulus, shear modulus, and Poisson ratio). The thermoelectric properties alongside the relaxation time were calculated with the BoltzTraP code [38]. These values are the average of the values obtained by the methods given by Voigt and Reuss [67,68].

3. Results and discussion

3.1. Mechanical properties of FeNbSb

This study applies the elastic constants got from Quantum Espresso to accurately predict the mechanical stability FeNbSb ternary alloy. From a material point of view, elastic constants are seen as suitable tools to model the mechanical behaviour of the material systems [39–43]. In addition, their mechanical properties have been examined through Quantum Espresso, and as such their elastic properties are depicted in Table 1. For elastic constants of cubic systems to predict the mechanical stability of materials, certain conditions [40] must be observed: $c_{11} = c_{22} = c_{33}, c_{12} = c_{23} = c_{13}, and\ c_{44} = c_{55} = c_{66}$. Other conditions [44,45] are: $c_{11} > 0, c_{44} > 0, c_{11} - c_{12} > 0, and\ c_{11} + 2c_{22} > 0$, where the shear constant ($c^{'} = c_{11} - c_{12}$) tells the nature of the system, in that if $c^{'}$ is negative then there is a presence of tetragonal distortion that causes the cubic phase unstable. But if $c^{'}$ is positive, then the cubic system is stable against the tetragonal phase. However, the positive value of $c^{'}$ of FeNbSb alloy in Table 1 is a sign that the system is free of tetragonal distortion. Also, the system shows high ductility because of its Cauchy pressure ($c^p = c_{11} - c_{12}$) is positive [41]. Interestingly the material of the study is not only ductile but malleable because its ratio of shear to bulk modulus in Table 1 is less than 0.571 [41–43,46]. Other indicators that scientifically testify that the material is ductile [47,48] and malleable are Pugh's ratio $\left(\frac{B}{G}\right) \rangle 1.75$ [49–51] and Poisson ratio $(n) > 0.26$ [52–54]. Since the literature validates that, this material is malleable and ductile, then its Debye temperature (θ_D) measures the lattice vibrational energies [46,55] to generate the highest normal modes of vibration in the material is significantly increased, as shown in Fig. 1. This is a signature of the presence of cohesive bonds (material's stiffness) among the atoms, which require the elevated temperature to cause an upward transition of phonon modes. In all, from the engineering point of view, FeNbSb is mechanically suitable for thermoelectricity.

3.2. Dynamical stability

Phonon dispersion spectra are known to comprise acoustic modes and optical modes. Both the formal and latter can be subdivided into transverse and longitudinal modes. These acoustic modes are differentiated from longitudinal modes by using n atoms in a unit cell, which means there are 3 acoustic modes while the $3n - 3$ degree of freedom relation corresponds to 6 optical modes. For a proper understanding of the dynamical stability of a crystal system, it is germane to critically examine its phonon dispersion spectra. Because phonon modes/spectra provide germane information about the stability of materials at $T > 0\ K$. However, the material becomes stable if the phonon modes (both optical and acoustic modes) are positive phonon frequencies otherwise the material becomes unstable (presence of negative phonon frequencies) [56]. For this study (as shown in Fig. 2), a finite displacement method has been carried out via a PHONOPY package [57] along with Quantum Espresso. From 2 we notice a small acoustic-optical gap between Γ and K points which may result in a weak interaction. Interestingly, a lower lattice thermal conductivity can be suggested at L a point because there exists a strong acoustic-optical interaction. Since literature has it that a low lattice thermal conductivity is a signature to an increase zT [58,59] then the FeNbSb system is suspected to have a higher figure of merit value.

3.3. Transport properties of FeNbSb

This study uses BoltzTraP software to calculate the Seebeck coefficient, electrical conductivity, and power factor. Fig. 3 shows how the transport properties depend on chemical potentials in the vicinity of $-1\ eV$ to $1\ eV$ at temperatures $300\ K \leq T \leq 800\ K$. The capacity of a material to have a very high power factor is one of the factors for

Table 1
Elastic properties of FeNbSb alloys.

HH	B (GPa)	G (GPa)	θ_D (K)	$\frac{B}{G}$	$\frac{G}{B}$	c^1	c^p	v_B (ms^{-1})	c_{11} (GPa)	c_{12} (GPa)	c_{44} (GPa)	v_G (ms^{-1})	v_P (ms^{-1})	n
FeNbSb	185	90.2	413	2.05	0.487	235	31	4584	342	106	75	3202	5889	0.29004

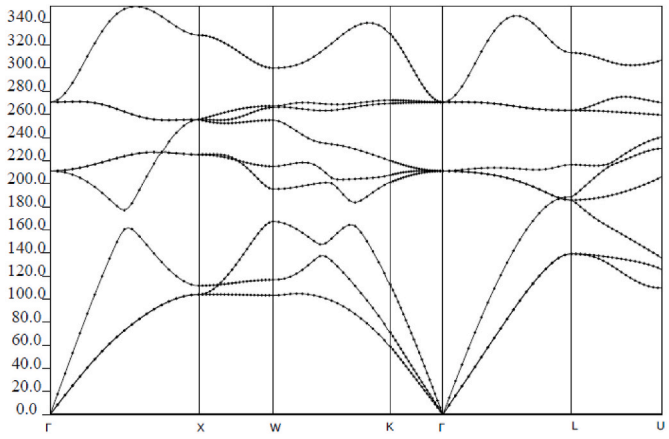

Fig. 2. Phonon dispersion curve of FeNbSb showing in (Hz).

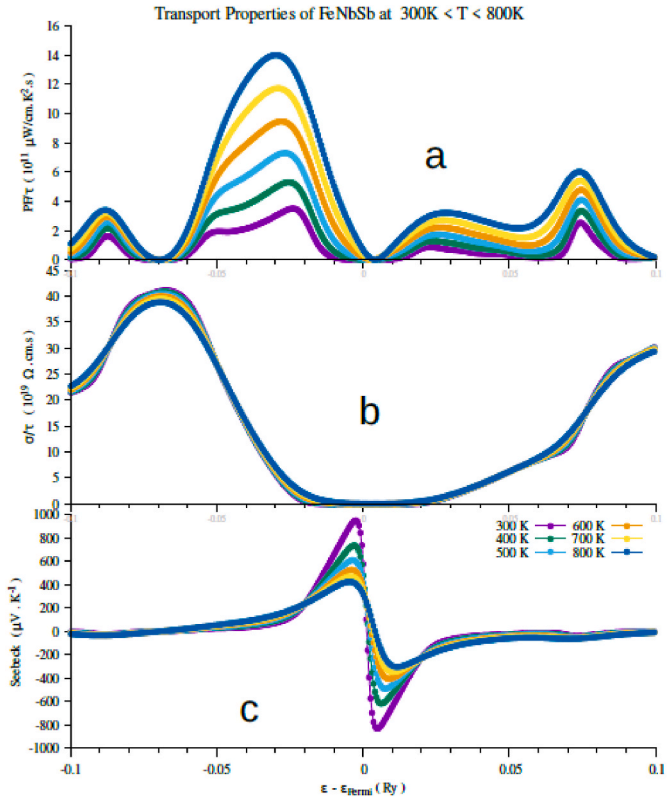

Fig. 3. Calculated values (a) Power factor (b) electronic thermal conductivity (c) Seebeck coefficient.

evaluating its thermoelectric usefulness. The material is more suitable for thermoelectricity the larger the power factor of such material. This study demonstrates that the power factor of FeNbSb alloy increases with temperature. The maximum power factor, $15 \times 10^{11}\ \mu W/cmK^2s$ is found in Fig. 3a at 800 K. Also, Fig. 3 (b) shows that its electrical conductivity is minimum at $\varepsilon - \varepsilon_F = 0$, and increases as $\varepsilon - \varepsilon_F$ increases. Also, the electrical conductivity of the p-type is greater than the n-type region,

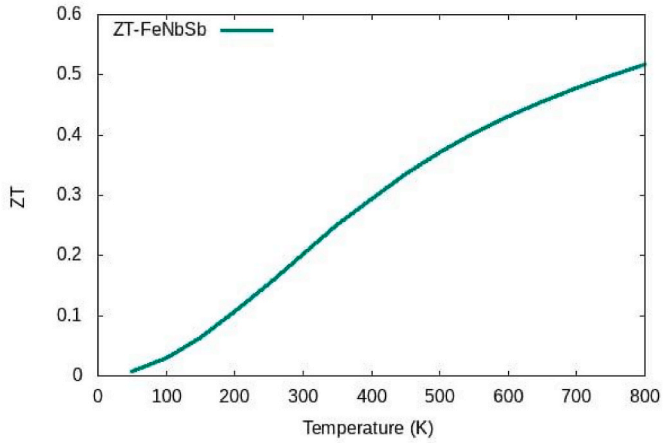

Fig. 4. Temperature as a function of figure of merit (zT) for half-Heusler *FeNbSb* compound.

and as such an increase in temperature has no effect. The Seebeck coefficient shows both P-type (positive trend) doping and N-type (negative trend) doping. The material with positive $\varepsilon - \varepsilon_F$ typifies the N-doping type while material with negative $\varepsilon - \varepsilon_F$ denotes P-type doping as shown in Fig. 3c. Whereas the possibility of using FeNbSb Heusler alloy for thermoelectricity was revealed from our results on the Seebeck coefficient, as presented in Fig. 3c. Here, we noticed that the Seebeck has the maximum and minimum values at room temperature. This implies that FeNbSb is a good candidate for thermolectric application. Moreover, the Seebeck coefficient of Fig. 3c shows an inverse relationship in that, the higher the temperature, the lower the Seebeck coefficient. It implies that the study has its highest Seebeck coefficient 850 μVK^{-1} for P-type and $-850\ \mu VK^{-1}$ for N-type at $\varepsilon - \varepsilon_F = -0.005$, $\varepsilon - \varepsilon_F = 0.005$, and, $T = 300\ K$. In addition, the figure of merit (zT) which determines the efficiency of thermoelectric material has its maximum value of 0.52 at 800 K for P-type *FeNbSb*. However, the result of this study is comparable with p-type *Sn* doped *FeNbSb* which has a maximum zT value of 0.66 at 923 K [60] and p-type $FeNb_{0.95}Ti_{0.05}Sb$ with a maximum zT value of 0.70 at 973 K [61] (see Fig. 4).

4. Conclusion

The structural, mechanical, vibrational and transport properties of FeNbSb have been examined via the first principle approach. The calculated elastic constants and phonon frequencies are signatures of the alloy is structurally stable and malleable as stated by Pugh's rule (B/G) and Poisson's ratio. The study recorded a higher power factor (because of its higher electrical conductivity) of $15 \times 10^{11}\ \mu W/cmK^2s$ and a maximum zT of 0.52 at 800 K in the p-type half-Heusler *FeNbSb*.

Declaration of competing interest

The authors declare that they have no known competing financial interests or personal relationships that could have appeared to influence the work reported in this paper.

References

[1] X.L. Shi, J. Zou, Z.G. Chen, Advanced thermoelectric design: from materials and structures to devices, Aug, Chem. Rev. 120 (15) (2020) 7399–7515, https://doi.org/10.1021/ACS.CHEMREV.0C00026/ASSET/IMAGES/MEDIUM/CR0C00026_0046.GIF.

[2] W. Liu, J. Hu, S. Zhang, M. Deng, C.G. Han, Y. Liu, New trends, strategies and opportunities in thermoelectric materials: a perspective, Mater. Today Phys. 1 (Jun. 2017) 50–60, https://doi.org/10.1016/J.MTPHYS.2017.06.001.

[3] Q. Zhang, et al., Deep defect level engineering: a strategy of optimizing the carrier concentration for high thermoelectric performance, Energy Environ. Sci. 11 (4) (Apr. 2018) 933–940, https://doi.org/10.1039/C8EE00112J.

[4] D.M. Rowe, Thermoelectrics, an environmentally-friendly source of electrical power, Renew. Energy 16 (1–4) (1999) 1251–1256, Jan, https://doi.org/10.1016/S0960-1481(98)00512-6.

[5] G.J. Snyder, E.S. Toberer, Complex thermoelectric materials, Nat. Mater. 7 (2) (Feb. 2008) 105–114, https://doi.org/10.1038/nmat2090, 2008 72.

[6] C. Fu, et al., Realizing high figure of merit in heavy-band p-type half-Heusler thermoelectric materials, Nat. Commun. 6 (1) (Sep. 2015) 1–7, https://doi.org/10.1038/ncomms9144, 2015 61.

[7] Y. Pei, X. Shi, A. Lalonde, H. Wang, L. Chen, G.J. Snyder, Convergence of electronic bands for high-performance bulk thermoelectrics, Nat 473 (7345) (May 2011) 66–69, https://doi.org/10.1038/nature09996, 2011 4737345.

[8] X. Liu, et al., Low electron scattering potentials in high-performance Mg2Si0.45Sn0.55 based thermoelectric solid solutions with band convergence, Adv. Energy Mater. 3 (9) (2013) 1238–1244, Sep, https://doi.org/10.1002/AENM.201300174.

[9] T.C. Harman, P.J. Taylor, M.P. Walsh, B.E. LaForge, Quantum dot superlattice thermoelectric materials and devices, Science 297 (5590) (2002) 2229–2232, https://doi.org/10.1126/SCIENCE.1072886. Sep.

[10] J.P. Heremans, et al., Enhancement of thermoelectric efficiency in PbTe by distortion of the electronic density of states, Science (80-.) 321 (5888) (Jul. 2008) 554–557, https://doi.org/10.1126/SCIENCE.1159725/SUPPL_FILE/HEREMANS_SOM.PDF.

[11] M. Hong, et al., Achieving zT > 2 in p-type AgSbTe2−xSex alloys via exploring the extra light valence band and introducing dense stacking faults, Adv. Energy Mater. 8 (9) (2018), 1702333, https://doi.org/10.1002/AENM.201702333. Mar.

[12] K. Zhao, et al., Solid-state explosive reaction for nanoporous bulk thermoelectric materials, Adv. Mater. 29 (42) (Nov. 2017), 1701148, https://doi.org/10.1002/ADMA.201701148.

[13] M. Hong, et al., N-type Bi2Te3-xSex nanoplates with enhanced thermoelectric efficiency driven by wide-frequency phonon scatterings and synergistic carrier scatterings, Apr, ACS Nano 10 (4) (2016) 4719–4727, https://doi.org/10.1021/ACSNANO.6B01156/SUPPL_FILE/NN6B01156_SI_001.PDF.

[14] L. Yang, Z.G. Chen, G. Han, M. Hong, Y. Zou, J. Zou, High-performance thermoelectric Cu2Se nanoplates through nanostructure engineering, Nano Energy 16 (Sep. 2015) 367–374, https://doi.org/10.1016/J.NANOEN.2015.07.012.

[15] Y. Pei, J. Lensch-Falk, E.S. Toberer, D.L. Medlin, G.J. Snyder, High thermoelectric performance in PbTe due to large nanoscale Ag2Te precipitates and La doping, Adv. Funct. Mater. 21 (2) (Jan. 2011) 241–249, https://doi.org/10.1002/ADFM.201000878.

[16] T. Graf, C. Felser, S.S.P. Parkin, Simple rules for the understanding of Heusler compounds, Prog. Solid State Chem. 39 (1) (May 2011) 1–50, https://doi.org/10.1016/J.PROGSOLIDSTCHEM.2011.02.001.

[17] T. Graf, S.S.P. Parkin, C. Felser, Heusler compounds - a material class with exceptional properties, IEEE Trans. Magn. 47 (2) (Feb. 2011) 367–373, https://doi.org/10.1109/TMAG.2010.2096229.

[18] J. Yang, H. Li, T. Wu, W. Zhang, L. Chen, J. Yang, Evaluation of half-heusler compounds as thermoelectric materials based on the calculated electrical transport properties, Adv. Funct. Mater. 18 (19) (Oct. 2008) 2880–2888, https://doi.org/10.1002/ADFM.200701369.

[19] H. Xie, et al., Beneficial contribution of alloy disorder to electron and phonon transport in half-heusler thermoelectric materials, Nov, Adv. Funct. Mater. 23 (41) (2013) 5123–5130, https://doi.org/10.1002/ADFM.201300663.

[20] S.R. Culp, J.W. Simonson, S.J. Poon, V. Ponnambalam, J. Edwards, T.M. Tritt, (Zr, Hf)Co(Sb, Sn) half-Heusler phases as high-temperature (>700°C) p-type thermoelectric materials, Appl. Phys. Lett. 93 (2) (Jul. 2008), 022105, https://doi.org/10.1063/1.2959103.

[21] C. Yu, T.J. Zhu, R.Z. Shi, Y. Zhang, X.B. Zhao, J. He, High-performance half-Heusler thermoelectric materials Hf1−x ZrxNiSn1−ySby prepared by levitation melting and spark plasma sintering, Acta Mater. 57 (9) (May 2009) 2757–2764, https://doi.org/10.1016/J.ACTAMAT.2009.02.026.

[22] C. Fu, T. Zhu, Y. Liu, H. Xie, X. Zhao, Band engineering of high-performance p-type FeNbSb based half-Heusler thermoelectric materials for the figure of merit zT > 1, Energy Environ. Sci. 8 (1) (Dec. 2014) 216–220, https://doi.org/10.1039/C4EE03042G.

[23] M. Schwall, B. Balke, Phase separation as a key to a thermoelectric high efficiency, Jan, Phys. Chem. Chem. Phys. 15 (6) (2013) 1868–1872, https://doi.org/10.1039/C2CP43946H.

[24] S. Chen, K.C. Lukas, W. Liu, C.P. Opeil, G. Chen, Z. Ren, Effect of Hf concentration on thermoelectric properties of nanostructured N-type half-heusler materials HfxZr1−xNiSn0.99Sb0.01, Sep, Adv. Energy Mater. 3 (9) (2013) 1210–1214, https://doi.org/10.1002/AENM.201300336.

[25] S. Chen, Z. Ren, Recent progress of half-Heusler for moderate temperature thermoelectric applications, Mater. Today 16 (10) (Oct. 2013) 387–395, https://doi.org/10.1016/J.MATTOD.2013.09.015.

[26] W. Xie, A. Weidenkaff, X. Tang, Q. Zhang, J. Poon, T.M. Tritt, Recent advances in nanostructured thermoelectric half-heusler compounds, Nanomaterials 2 (4) (Dec. 2012) 379, https://doi.org/10.3390/NANO2040379.

[27] J. Schmitt, Z.M. Gibbs, G.J. Snyder, C. Felser, Resolving the true band gap of ZrNiSn half-Heusler thermoelectric materials, Mater. Horiz. 2 (1) (Dec. 2014) 68–75, https://doi.org/10.1039/C4MH00142G.

[28] G. Joshi, et al., NbFeSb-based p-type half-Heuslers for power generation applications, Nov, Energy Environ. Sci. 7 (12) (2014) 4070–4076, https://doi.org/10.1039/C4EE02180K.

[29] F.J. Disalvo, Thermoelectric cooling and power generation, Science (80-.) 285 (5428) (Jul. 1999) 703–706, https://doi.org/10.1126/SCIENCE.285.5428.703.

[30] A.J. Minnich, M.S. Dresselhaus, Z.F. Ren, G. Chen, Bulk nanostructured thermoelectric materials: current research and future prospects, Energy Environ. Sci. 2 (5) (May 2009) 466–479, https://doi.org/10.1039/B822664B.

[31] W. Liu, X. Yan, G. Chen, Z. Ren, Recent advances in thermoelectric nanocomposites, Nano Energy 1 (1) (Jan. 2012) 42–56, https://doi.org/10.1016/J.NANOEN.2011.10.001.

[32] P. Giannozzi, et al., Quantum espresso: a modular and open-source software project for quantum simulations of materials, J. Phys. Condens. Matter 21 (39) (Sep. 2009), 395502, https://doi.org/10.1088/0953-8984/21/39/395502.

[33] J.P. Perdew, K. Burke, M. Ernzerhof, Generalized gradient approximation made simple, Phys. Rev. Lett. 77 (18) (1996) 3865–3868, https://doi.org/10.1103/PHYSREVLETT.77.3865.

[34] H.J. Monkhorst, J.D. Pack, Special points for Brillouin-zone integrations, Phys. Rev. B 13 (12) (1976) 5188, https://doi.org/10.1103/PhysRevB.13.5188. Jun.

[35] W. Voigt, Ueber die Beziehung zwischen den beiden Elasticitätsconstanten isotroper Körper, Ann. Phys. 274 (12) (Jan. 1889) 573–587, https://doi.org/10.1002/ANDP.18892741206.

[36] A. Reuss, Berechnung der Fließgrenze von Mischkristallen auf Grund der Plastizitätsbedingung für Einkristalle, ZAMM - J. Appl. Math. Mech./Z. Angew. Math. Mech. 9 (1) (Jan. 1929) 49–58, https://doi.org/10.1002/ZAMM.19290090104.

[37] R. Hill, The elastic behaviour of a crystalline aggregate, Proc. Phys. Soc. A 65 (5) (May 1952) 349, https://doi.org/10.1088/0370-1298/65/5/307.

[38] G.K.H. Madsen, D.J. Singh, BoltzTraP. A code for calculating band-structure dependent quantities, Comput. Phys. Commun. 175 (1) (2006) 67–71, https://doi.org/10.1016/J.CPC.2006.03.007. Jul.

[39] R. Dutt, D. Pandey, A. Chakrabarti, Probing the martensite transition and thermoelectric properties of Cox TaZ (Z= Si, Ge, Sn and x = 1, 2): a study based on density functional theory, J. Phys. Condens. Matter 33 (4) (Oct. 2020), 45402, https://doi.org/10.1088/1361-648X/ABBB40.

[40] F. Mouhat, F.X. Coudert, Necessary and sufficient elastic stability conditions in various crystal systems, Phys. Rev. B 90 (22) (2014), 224104, https://doi.org/10.1103/PhysRevB.90.224104. Dec.

[41] W. Everhart, J. Newkirk, Mechanical properties of Heusler alloys, Heliyon 5 (5) (May 2019), https://doi.org/10.1016/J.HELIYON.2019.E01578.

[42] T. Roy, M.E. Gruner, P. Entel, A. Chakrabarti, Effect of substitution on elastic stability, electronic structure and magnetic property of Ni–Mn-based Heusler alloys: an ab initio comparison, J. Alloys Compd. 632 (May 2015) 822–829, https://doi.org/10.1016/J.JALLCOM.2015.01.255.

[43] T. Roy, A. Chakrabarti, Ab initio studies on electronic and magnetic properties of X2PtGa (X=Cr, Mn, Fe, Co) Heusler alloys, J. Magn. Magn Mater. 423 (Feb. 2017) 395–404, https://doi.org/10.1016/J.JMMM.2016.09.127.

[44] M. Born, On the stability of crystal lattices. I, Math. Proc. Camb. Phil. Soc. 36 (2) (1940) 160–172, https://doi.org/10.1017/S0305004100017138.

[45] M. Born, K. Huang, M. Lax, Dynamical theory of crystal lattices, Am. J. Phys. 23 (7) (2005) 474, https://doi.org/10.1119/1.1934059. Jul.

[46] H.M. Ledbetter, R.P. Reed, Elastic properties of metals and alloys, I. Iron, nickel, and iron-nickel alloys, J. Phys. Chem. Ref. Data 2 (3) (Oct. 2009) 531, https://doi.org/10.1063/1.3253127.

[47] B. Fadila, et al., Structural, magnetic, electronic and mechanical properties of full-Heusler alloys Co2YAl (Y = Fe, Ti): first-principles calculations with different exchange-correlation potentials, J. Magn. Magn Mater. 448 (Feb. 2018) 208–220, https://doi.org/10.1016/J.JMMM.2017.06.048.

[48] F. Parvin, S.H. Naqib, Pressure dependence of structural, elastic, electronic, thermodynamic, and optical properties of van der Waals-type NaSn2P2 pnictide superconductor: insights from DFT study, Results Phys. 21 (Feb. 2021), 103848, https://doi.org/10.1016/J.RINP.2021.103848.

[49] K. Akter, F. Parvin, M.A. Hadi, A.K.M.A. Islam, Insights into the predicted Hf2SN in comparison with the synthesized MAX phase Hf2SC: a comprehensive study, Comput. Condens. Matter 24 (Sep. 2020), e00485, https://doi.org/10.1016/J.COCOM.2020.E00485.

[50] A. Moussali, M.B. Amina, B. Fassi, I. Ameri, M. Ameri, Y. Al-Douri, First-principles calculations to investigate structural and thermodynamic properties of Ni2Laz (Z = As, Sb and Bi) Heusler alloys, Indian J. Phys. 94 (11) (Nov. 2019) 1733–1747, https://doi.org/10.1007/S12648-019-01627-Z, 2019 9411.

[51] Z. Souadia, A. Bouhemadou, R. Khenata, Y. Al-Douri, Structural, elastic and lattice dynamical properties of the alkali metal tellurides: first-principles study, Phys. B Condens. Matter 521 (Sep. 2017) 204–214, https://doi.org/10.1016/J.PHYSB.2017.07.004.

[52] M.A. Alam, M. Nuruzzaman, M.A.H. Shah, F. Parvin, M.A.K. Zilani, Structural, mechanical, electronic and thermal properties of the newly predicted NB2 from ab initio calculations, Dec, Chin. J. Phys. 55 (6) (2017) 2540–2547, https://doi.org/10.1016/J.CJPH.2017.08.029.

[53] G. Vaitheeswaran, V. Kanchana, A. Svane, A. Delin, Elastic properties of MgCNi3—a superconducting perovskite, J. Phys. Condens. Matter 19 (32) (Jul. 2007), 326214, https://doi.org/10.1088/0953-8984/19/32/326214.
[54] O.L. Anderson, H.H. Demarest, Elastic constants of the central force model for cubic structures: polycrystalline aggregates and instabilities, J. Geophys. Res. 76 (5) (Feb. 1971) 1349–1369, https://doi.org/10.1029/JB076I005P01349.
[55] R. Dutt, J. Bhattacharya, A. Chakrabarti, Investigation of mechanical, lattice dynamical, electronic and thermoelectric properties of half Heusler chalcogenides: a DFT study, J. Phys. Chem. Solid. 167 (Aug. 2022), 110704, https://doi.org/10.1016/J.JPCS.2022.110704.
[56] G. Grimvall, B. Magyari-Köpe, E.N.M. Ozoliņ, K.A. Persson, Lattice instabilities in metallic elements, Rev. Mod. Phys. 84 (2) (Jun. 2012) 945–986, https://doi.org/10.1103/REVMODPHYS.84.945.
[57] L. Chaput, A. Togo, I. Tanaka, G. Hug, Phonon-phonon interactions in transition metals, Phys. Rev. B Condens. Matter 84 (9) (Sep. 2011), 94302, https://doi.org/10.1103/PHYSREVB.84.094302/FIGURES/4/MEDIUM.
[58] L. Hu, et al., High thermoelectric performance enabled by the convergence of nested conduction bands in Pb7Bi4Se13 with low thermal conductivity, Nat. Commun. 12 (1) (Aug. 2021) 1–10, https://doi.org/10.1038/s41467-021-25119-z, 2021 121.
[59] A. Mehdizadeh Dehkordi, M. Zebarjadi, J. He, T.M. Tritt, Thermoelectric power factor: enhancement mechanisms and strategies for higher performance thermoelectric materials, Mater. Sci. Eng. R Rep. 97 (Nov. 2015) 1–22, https://doi.org/10.1016/J.MSER.2015.08.001.
[60] L. Yue, et al., Sn doped FeNbSb half-heusler compounds for tuning thermoelectric performance, J. Electron. Mater. 49 (5) (Jan. 2020) 2862–2871, https://doi.org/10.1007/S11664-019-07919-8, 2020 495.
[61] R. He, et al., Achieving high power factor and output power density in p-type half-Heuslers Nb1-xTixFeSb, Proc. Natl. Acad. Sci. U.S.A. 113 (48) (Nov. 2016) 13576–13581, https://doi.org/10.1073/PNAS.1617663113/SUPPL_FILE/PNAS.201617663SI.PDF.